Am J Physiol Heart Circ Physiol 297: H1398–H1410, 2009.
First published July 24, 2009; doi:10.1152/ajpheart.00411.2009.

K^+ current changes account for the rate dependence of the action potential in the human atrial myocyte

Mary M. Maleckar,[1,2] Joseph L. Greenstein,[1] Wayne R. Giles,[3] and Natalia A. Trayanova[1]

[1]*Department of Biomedical Engineering and Institute for Computational Medicine, Johns Hopkins University, Baltimore, Maryland;* [2]*Center for Biomedical Computing, Simula Research Laboratory, Oslo, Norway; and* [3]*Faculty of Kinesiology, University of Calgary, Calgary, Alberta, Canada*

Submitted 4 May 2009; accepted in final form 20 July 2009

Maleckar MM, Greenstein JL, Giles WR, Trayanova NA. K^+ current changes account for the rate dependence of the action potential in the human atrial myocyte. *Am J Physiol Heart Circ Physiol* 297: H1398–H1410, 2009. First published July 24, 2009; doi:10.1152/ajpheart.00411.2009.—Ongoing investigation of the electrophysiology and pathophysiology of the human atria requires an accurate representation of the membrane dynamics of the human atrial myocyte. However, existing models of the human atrial myocyte action potential do not accurately reproduce experimental observations with respect to the kinetics of key repolarizing currents or rate dependence of the action potential and fail to properly enforce charge conservation, an essential characteristic in any model of the cardiac membrane. In addition, recent advances in experimental methods have resulted in new data regarding the kinetics of repolarizing currents in the human atria. The goal of this study was to develop a new model of the human atrial action potential, based on the Nygren et al. model of the human atrial myocyte and newly available experimental data, that ensures an accurate representation of repolarization processes and reproduction of action potential rate dependence and enforces charge conservation. Specifically, the transient outward K^+ current (I_t) and ultrarapid rectifier K^+ current (I_{Kur}) were newly formulated. The inwardly recitifying K^+ current (I_{K1}) was also reanalyzed and implemented appropriately. Simulations of the human atrial myocyte action potential with this new model demonstrated that early repolarization is dependent on the relative conductances of I_t and I_{Kur}, whereas densities of both I_{Kur} and I_{K1} underlie later repolarization. In addition, this model reproduces experimental measurements of rate dependence of I_t, I_{Kur}, and action potential duration. This new model constitutes an improved representation of excitability and repolarization reserve in the human atrial myocyte and, therefore, provides a useful computational tool for future studies involving the human atrium in both health and disease.

ionic model; repolarization; potassium current

ACCURATE REPRESENTATION of the ionic currents of the human atrial myocyte is essential for the ongoing investigation of human atrial electrophysiology and pathophysiology. It is now well established that the elucidation of mechanisms underlying the complex phenomena that occur in highly integrative systems, such as atrial tissue, requires that experimental data be incorporated such that models are both accurate and biophysically based.Within the past decade, advances in experimental methods have resulted in a much-improved characterization of repolarizing currents in the human atria (21, 50, 59–61). New insights into the underlying channel isoforms responsible for these K^+ currents are also now available (32, 41, 53, 54, 56). However, findings regarding essential repolarization processes in the human atria have been incorporated into none of the available mathematical models of the action potential (AP) (7, 40).

Of particular interest are the recent experimental findings regarding the transient outward K^+ current (I_t; $K_v4.3$) and ultrarapid delayed rectifier K^+ current (I_{Kur}; $K_v1.5$). I_t contributes significantly to the early repolarization phase of the human atrial AP, which is analogous to its contribution to phase 1 repolarization in human ventricular myocytes. I_{Kur}, a sustained outward current that is expressed in human atrial but not ventricular myocytes, contributes to both early and late repolarization in the human atrial myocyte. The rapid and slow delayed rectifier K^+ currents (I_{Kr} and I_{Ks}, respectively), which are essential for late repolarization in the human ventricle, are very small (or even undetectable) in the human atria (18). The inward rectifier K^+ current (I_{K1}), which contributes to late repolarization and stabilizes the resting membrane potential (RMP), is expressed at a much lower density in the human atria compared with the ventricles; I_{K1} has been measured in the human atria at densities that are 10–50% of those found in the human ventricle (30).

The main goals of the present study were twofold: *1*) to create a new model of the human atrial AP that accurately represents repolarization in the human atrial myocyte, which will be accomplished by the reformulation of I_t and I_{Kur}, and *2*) to analyze the contribution of repolarization processes to the rate dependence of the human atrial AP. The result was a well-quantified model of the human atrial myocyte that ensures the availability of a physiologically relevant and robust model for cell-, tissue-, and, eventually, organ-level studies of atrial electrophysiological phenomena, including arrhythmogenesis.

Glossary

a_{ur}	Activation gating variable for I_{Kur}
AP	Action potential
APD	AP duration
APD_{20}	APD at 20% repolariation
APD_{30}	APD at 30% repolarization
APD_{90}	APD at 90% repolarization
$[Ca^{2+}]_c$	Ca^{2+} concentration in the extracellular cleft space
$[Ca^{2+}]_d$	Ca^{2+} concentration in the restricted subsarcolemmal space
$[Ca^{2+}]_i$	Intracellular Ca^{2+} concentration
$[Ca^{2+}]_{rel}$	Ca^{2+} concentration in the sarcoplasmic reticulum release compartment
$[Ca^{2+}]_{up}$	Ca^{2+} concentration in the sarcoplasmic reticulum uptake compartment

Address for reprint requests and other correspondence: M. M. Maleckar, PO Box 134, Lysaker 1325, Norway (e-mail: mmaleck@simula.no).

C_m	Cell capacitance
d_L	Activation gating variable for $I_{Ca,L}$
dV/dt_{max}	Maximum upstroke velocity
E_K	Equilibrium (Nernst) potential for K^+
f_{L1}	Fast inactivation gating variable for $I_{Ca,L}$
f_{L2}	Slow inactivation gating variable for $I_{Ca,L}$
F	Faraday's constant
F_1	Relative amount of "inactive precursor" in the I_{rel} formulation
F_2	Relative amount of "activator" in the I_{rel} formulation
g_{Kur}	Maximum conductance for I_{Kur}
g_t	Maximum conductance for I_t
g_{K1}	Maximum conductance for I_{K1}
h_1	Fast inactivation variable for I_{Na}
h_2	Slow inactivation variable for I_{Na}
hAMr model	Human atrial myocyte with new repolarization model
i_{ur}	Inactivation gating variable for I_{Kur}
I_{BCa}	Background Ca^{2+} current
I_{BNa}	Background Na^+ current
$I_{Ca,L}$	L-type Ca^{2+} current
I_{CaP}	Ca^{2+} pump current, sarcolemmal
I_{K1}	Inwardly rectifying K^+ current
$I_{K(ACh)}$	ACh-sensitive K^+ current
I_{Kr}	Rapid delayed rectifier K^+ current (human *ether-a-go-go*-related gene)
I_{Ks}	Slow delayed rectifier K^+ current
I_{Kur}	Ultrarapid delayed rectifier K^+ current
I_{Na}	Na^+ current
I_{NaCa}	Na^+/Ca^{2+} exchange current
I_{NaK}	Na^+-K^+ pump current, sarcolemmal
$I_{NaK,max}$	Maximum Na^+-K^+ pump current
I_{stim}	Stimulus current
I_t	Transient outward K^+ current
k_{Ca}	Half-maximum Ca^{2+} binding concentration for f_{Ca}
$[K^+]_c$	K^+ concentration in the extracellular cleft space
$[K^+]_i$	Intracellular K^+ concentration
m	Activation gating variable for I_{Na}
n	Activation gating variable for I_{Ks}
$[Na^+]_c$	Na^+ concentration in the extracellular cleft space
$[Na^+]_i$	Intracellular Na^+ concentration
O_C	Fractional occupancy of the calmodulin-Ca^{2+} buffer by Ca^{2+}
O_{Calse}	Fractional occupancy of the calsequestrin-Ca^{2+} buffer by Ca^{2+}
O_{TC}	Fractional occupancy of the troponin-Ca^{2+} buffer by Ca^{2+}
O_{TMgC}	Fractional occupancy of the troponin-Mg^{2+} buffer by Ca^{2+}
O_{TMgMg}	Fractional occupancy of the troponin-Mg^{2+} buffer by Mg^{2+}
p_a	Activation gating variable for I_{Kr}
P_{Na}	Permeability for I_{Na}
r	Activation gating variable for I_t
R	Universal gas constant
RMP	Resting membrane potential
s	Inactivation gating variable for I_t
T	Absolute temperature
V	Membrane voltage
Vol_i	Total myocyte volume
$\Phi_{Na,en}$	Electroneutral Na^+ influx
τ_{aur}	Activation time constant for I_{Kur}
τ_{iur}	Inactivation time constant for I_{Kur}
τ_r	Activation time constant for I_t
τ_s	Inactivation time constant for I_t

METHODS

Basic Assumptions

Many fundamental aspects of the mathematical model presented in this article are based on a previous model of the adult human atrial myocyte AP, that of Nygren et al. (40). Our model will be referred to as the human atrial myocyte with new repolarization (hAMr) model. It consists of an electric equivalent circuit for the sarcolemma, including ionic currents based on Hodgkin-Huxley formalisms, as well as a fluid compartment model to account for changes in ionic concentrations, as described previously (40). The dimensions and capacitance of the human atrial myocyte are the same as those in the original article (40); specifically, total myocyte volume (Vol_i) and cell membrane capacitance (C_m) were considered to be 5.884 μl and 50 pF, respecitively.

Transmembrane Ionic Currents

Figure 1 is a schematic of the hAMr model of the human atrial myocyte. The formulation includes all time- and voltage-dependent ion currents that contribute to the generation of the human atrial AP: the Na^+ current (I_{Na}), the L-type Ca^{2+} current ($I_{Ca,L}$), and the K^+ currents I_t, I_{Kur}, I_{K1}, I_{Kr}, and I_{Ks}. In addition, our model includes electrogenic pump and exchanger currents: the sarcolemmal Ca^{2+} pump currrent ($I_{Ca,P}$), the Na^+/Ca^{2+} exchanger current (I_{NaCa}), and the Na^+-K^+ pump current (I_{NaK}), which are responsible for the maintenance of intracellular ion concentrations. Na^+ and Ca^{2+} time-independent or background currents (I_{BNa} and I_{BCa}, respectively) are also included. The K^+ currents that are the focus of the present study, I_t, I_{Kur}, and I_{K1}, are shown in bold and indicated by the dashed ellipse in Fig. 1; the formulations of the remaining currents and ion fluxes are

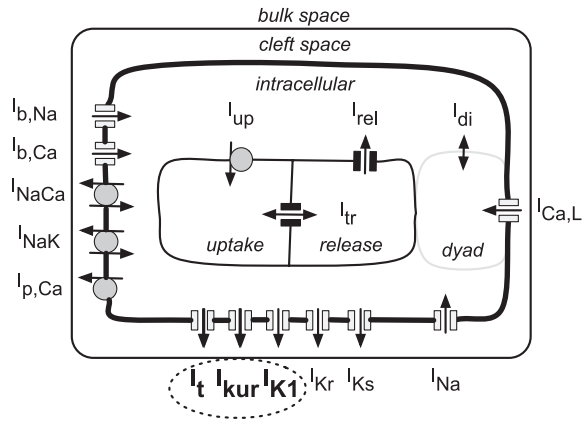

Fig. 1. Schematic representation of the mathematical model of the human atrial myocyte (hAMr model). Ion channel-mediated currents as well as electrogenic pump and ion exchanger currents are shown. Significant compartments include the extracellular, intracellular, and cleft spaces as well as the uptake and release compartments within the sarcoplasmic reticulum (40). The dashed ellipse indicates the currents that are the main focus of this new model of the human atrial AP. The myocyte was modeled as a cylindrical cell with a length of 130 μm and a diameter of 11 μm. Cell capacitance was 50 pF. See the *Glossary* for definitions of abbreviations used in this and subsequent figures.

based on the formulation of Ref. 40, with some parameters updated. In the present model, I_t and I_{Kur} are the transient and sustained components, respectively, of the outward K^+ current. The significant reformulation and novel contribution of these key repolarization currents are described in detail in the next two sections.

I_t

Due to a lack of experimental data, the Nygren et al. (40) formulation of I_t in the human atrial myocyte was based on experimental data obtained from rabbit atrial myocytes (16). It is now well accepted that the K^+ channel underlying I_t in the rabbit atria is the $K_v1.4$ gene product, whereas in the human atria, the α-subunit encoded by $K_v4.3$ underlies this current (14, 16, 42, 53, 54, 56). In human atria, I_t activates very rapidly (~10 ms) (46) and then inactivates more slowly (~20 ms) (56). The recovery from inactivation is strongly voltage dependent (56) and relatively rapid (on the order of 10s of ms) (55, 56). In contrast, in the model of Nygren et al. (40), the time course of recovery was on the order of ~300 ms at hyperpolarized potentials.

Figure 2 shows the new implementation of I_t in the hAMr model. Figure 2*A* shows implementations made to achieve improved kinetic descriptions for the time constant of inactivation (τ_s). These were based on newer experimental data from the human atrium (56). Figure 2*B* shows a family of current traces of I_t generated by our new formulation when subjected to the voltage-clamp protocol shown in the *inset*; note that the current is both rapidly activating and inactivating. Figure 2, *C* and *D*, compare current traces generated by the hAMr model and the model of Nygren et al. when subjected to identical voltage clamps from −80 to −20 and +20 mV, respectively (as indicated in the *insets*). Note the more rapid decay of the updated I_t compared with the same current in the model of Nygren et al. for negative (Fig. 2*C*) versus positive (Fig. 2*D*) holding potentials. A complete mathematical description of the new formulation of I_t can be found in the APPENDIX.

I_{Kur}

In the Nygren et al. (40) model of the human atrial myocyte AP, recovery from inactivation of the "sustained outward K^+ current" (I_{sus}) was represented via a time course on the order of ~300 ms and included a partial inactivation of 40%. I_{sus} is now known to be I_{Kur}, a member of the family of ultrarapidly delayed rectifier K^+ currents encoded by the $K_v1.5$ gene (13). I_{Kur} activates very rapidly (<10 ms) (1) and inactivates very slowly (~3 s) but completely.

Figure 3 shows the major changes to I_{Kur} made to accurately simulate the kinetics of inactivation and recovery of this current. Figure 3*A* shows the new implementations of the steady-state activation and inactivation of I_{Kur}. Steady-state activation was adjusted to match data from human atrial myocytes (13). The partial steady-state inactivation present in the original model (40) was replaced by a complete inactivation process in the hAMr model (58). Figure 3*B* shows the new voltage dependence of the time constant of inactivation at hyperpolarized potentials; it was increased by ~10-fold (15) (Fig. 3*B*, *top*, solid black trace). Figure 3*C* shows current traces of I_{Kur} generated by the voltage clamp steps shown in the *inset*. For holding potentials of ±20 mV, current traces of I_{sus}, the analogous current from the model of Nygren et al., are also shown for comparison (Fig. 3*C*, dashed traces); note that I_{sus} decays much more rapidly compared with I_{Kur}. A comparison of the sum of I_t and I_{Kur} elicited via the voltage-clamp protocol shown in the *inset* revealed a close correspondence between the recent experiment (Fig. 3*D*, *top*) (21) and hAMr model (Fig. 3*D*, *bottom*). A complete mathematical description of the formulation of I_{Kur} in the present model can be found in the APPENDIX.

Optimization of Parameters

Individual parameter values in each mathematical formulation in the hAMr model were optimized to reproduce physiologically relevant experimental observations. The specific magnitudes of these changes are discussed in the following section; two prime examples are I_{K1} and I_{Na}. Please reference the APPENDIX for the exact parameter values.

I_{K1}

While the mathematical formulation of I_{K1} remains the same as in Ref. 40, the maximum conductance of I_{K1} (g_{K1}) was increased by ~3%; this change maintains the RMP at experimentally measured

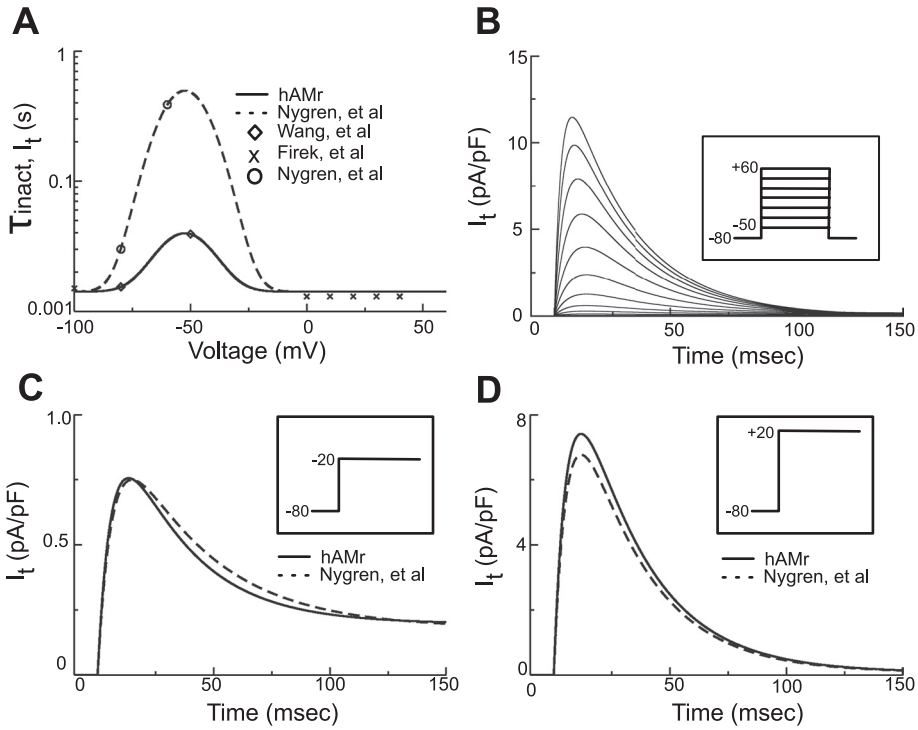

Fig. 2. Modification of I_t. *A*: data describing the modification of voltage-dependent kinetics of reactivation in Ref. 40 (○). The time constant of inactivation/recovery (τ_{inact}) is shown by the dashed trace. The present model is based on more complex recovery data [◇ (56)]. This, combined with inactivation data ["X"s (18)], led to a new formulation for the time constant of inactivation/recovery in the hAMr model (solid trace). *B*: a family of current recordings of I_t simulated using a holding potential of −80 mV and a series of 750-ms voltage clamp steps from −50 to +60 mV in 10-mV increments applied at 0.1 Hz (as shown in the *inset*). *C*: simulated currents after a voltage clamp step from a holding potential of −80 to −20 mV (as shown in the *inset*) for the hAMr model (solid trace) and the model of Nygren et al. (dashed trace). *D*: simulated currents after a voltage clamp step from a holding potential of −80 to +20 mV (as shown in the *inset*) for the hAMr model (solid trace) and the model of Nygren et al. (dashed trace).

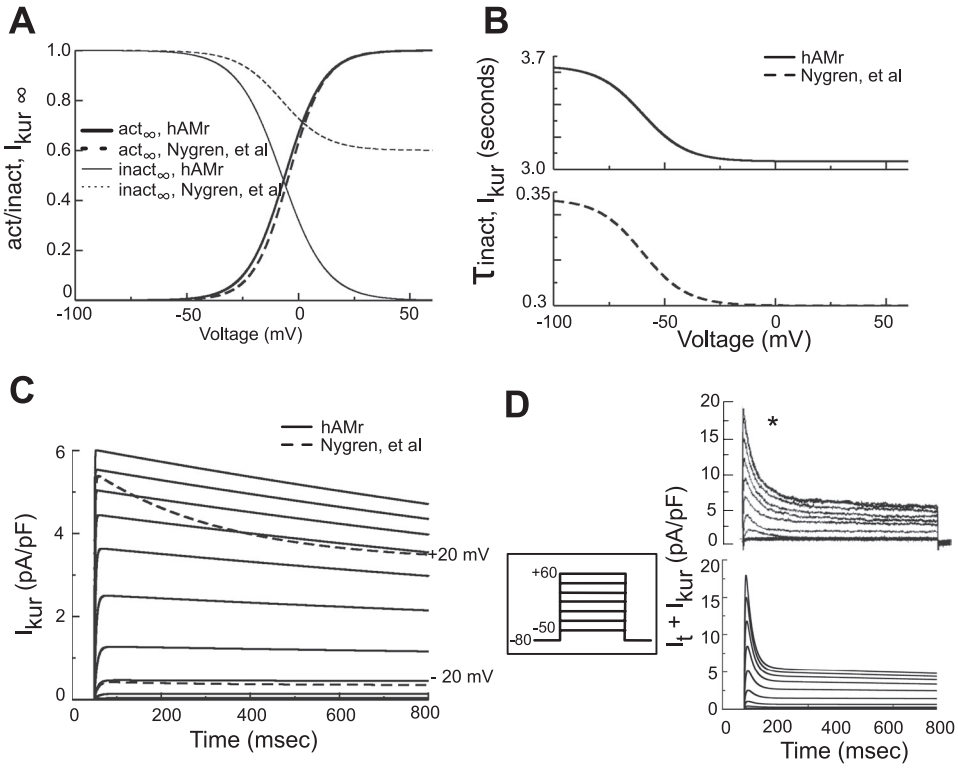

Fig. 3. Modification of I_{Kur}. *A*: steady-state activation and inactivation variables for I_{Kur}. Parameters for both the Nygren et al. and hAMr models are shown. *B*: time constants for the inactivation of I_{Kur} for the hAMr model (*top*) and the model of Nygren et al. (*bottom*). *C*: current traces of I_{Kur} (solid traces) simulated using a holding potential of −80 mV and a series of 750-ms-duration depolarizing steps from −50 to +60 mV applied in 10-mV increments (as shown in the *inset* between *C* and *D*). Additionally, for depolarizing steps to −20 and +20 mV, simulated current traces of I_{sus}, the analogous current in the model of Nygren et al., are overlaid for comparison (dashed traces). *D*: a family of currents corresponding to the sum of I_t and I_{Kur} recorded from experiments [*top* [*Reprinted from *Eur J Pharmacol* 497, Gluais P. et al. (21), Risperidone reduces K^+ currents in human atrial myocytes and prolongs repolarization in human myocardium, p. 215–222, 2004, with permission of Elsevier. Permission also granted by authors (21)]. These results were compared with the same simulated traces (*bottom*) generated by an identical voltage-clamp protocol in silico (shown in the *inset* between *C* and *D*).

values and results in I_{K1} densities within the range of experimentally validated values for the human atria (59, 61).

I_{Na}

It was necessary to increase the peak magnitude of this current by 12.5% by adjusting the Na^+ permeability (P_{Na}) to agree with experimental measurements of the maximum upstroke velocity (dV/dt_{max}) of the human atrial AP. Specifically, this change increased dV/dt_{max} from ~120 to ~150 V/s when stimulated at 1.5 times the threshold for activation, which falls within the experimentally measured range of values for human atrial myocytes (8).

I_t and I_{Kur}

The maximum conductance of I_t (g_t) was increased by ~9% in the hAMr model to match values reported in recent experiments (21, 60). The maximum channel conductance of I_{Kur} (g_{Kur}) was decreased by ~11% in the hAMr model to fit recent experimental data (21).

Material Balance: Elimination of the Electroneutral Na^+ Influx

The model of Nygren et al. (40) incorporated an electroneutral Na^+ influx (Φ_{en}) to achieve long-term stability in ionic concentrations over long periods of stimulation at a specific rate (1 Hz) and stimulus strength (280 pA, or 5.6 pA/pF). A consequence of the incorporation of this flux is a lack of charge conservation as well as the absence of any true mathematical steady states (25). These factors limit the ability of any model to accurately reproduce long-term physiological phenomena and thus decrease its predictive power. In the hAMr model, Φ_{en} was removed, and the stimulus current delivered to the intracellular space was attributed to the influx of potassium ions, as suggested by Hund et. al. (24). As a result, charge is conserved within the system for the hAMr model for any stimulation protocol.

RESULTS

The simulation results presented here had two goals: *1*) to illustrate the effects of incorporation of essential new K^+ current data and *2*) to further explore the mechanisms underlying the repolarization reserve in the human atrial myocyteby by examining both early and late repolarizationin in the hAMr model.

RMP

A detailed understanding of the factors that control the RMP is one of the essential elements of any physiologically accurate model (33). This reflects a dynamic balance between the time-independent background, pump, and exchanger currents (I_{K1}, $I_{B,Na}$, $I_{B,Ca}$, I_{NaK}, I_{CaP}, and I_{NaCa}). In Fig. 4*A*, the current-voltage relationships of five of the key ion-trafficking mechanisms that are responsible for determining the RMP in the quiescent atrial myocyte (I_{K1}, I_{NaCa}, I_{NaK}, $I_{B,Ca}$, and $I_{B,Na}$) are shown. The resulting net current and RMP in our model are also shown. As indicated by the arrows, the net membrane current is zero at approximately −74.0 mV, in agreement with experimental measurements of the RMP (8, 12, 20, 46, 52). We note that RMP exhibits strong dependence on I_{K1}; for example, a 10% increase in this conductance (g_{K1}) will cause a decrease in RMP of ~1 mV in the absence of other alterations in the hAMr model. The dependence of the RMP on g_{K1} for a wider range of conductances is shown in Fig. 4*B*.

Long-Term Steady State of Simulated Ion Fluxes

The long-term steady-state ionic concentrations in our model are shown in Fig. 5 for pacing rates of 1 and 2 Hz and for a simulation time of 10 min (600 and 1,200 cycles, respectively). Initial conditions for pacing at both rates were steady-state values following pacing at a rate of 1 Hz. The cleft concentrations of K^+, Ca^{2+}, and Na^+ (Fig. 5, *A*, *C*, and *E*, respectively, solid traces) showed steady-state ionic balance through the entire time course of stimulation at a pacing rate of 1 Hz.

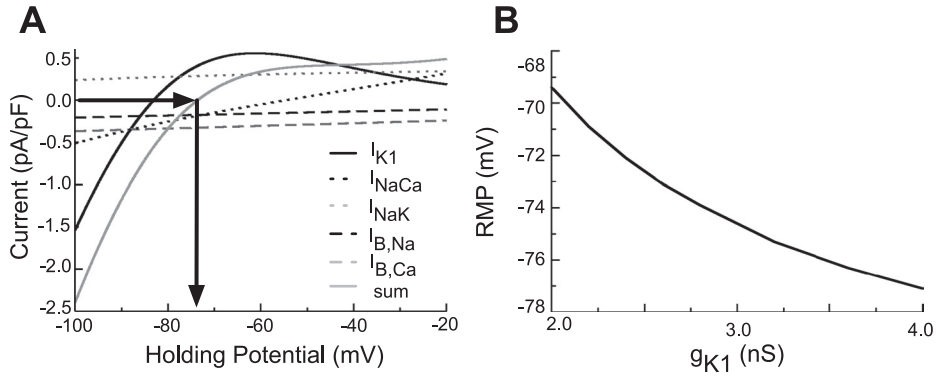

Fig. 4. *A*: current-voltage relationships of the currents underlying the stability of RMP (I_{K1}, I_{NaCa}, and $I_{B,Na}$) in the hAMr model along with the sum of these currents (solid shaded trace), which can be used to predict the RMP of the model. *B*: examination of the sensitivity of RMP to changes in g_{K1}.

When the pacing rate was elevated to 2 Hz (Fig. 5, *A*, *C*, and *E*, shaded traces), the cleft concentrations initially changed somewhat. $[K^+]_c$ initially rose by ~1 mmol/l and then returned to a steady-state value as a result of I_{NaK} activity and diffusion, consistent with experimental observations (31). The intracellular concentrations of K^+, Ca^{2+}, and Na^+ (Fig. 5, *B*, *D*, and *F*, respectively, solid traces) also demonstrated steady-state ionic balance through the entire time course of stimulation at a pacing rate of 1 Hz. When the pacing rate was elevated to 2 Hz, $[K^+]_i$ and $[Na^+]_i$ (Fig. 5, B and F, respectively, shaded traces) reached steady state within the time course of simulation, decreasing by 2.0 mmol/l and increasing by 1.5 mmol/l, respectively. The peak magnitude of $[Ca^{2+}]_i$ (Fig. 5*D*, shaded trace) decreased slightly by 0.1 μmol/l at steady state for pacing at 2 Hz, and diastolic $[Ca^{2+}]_i$ increased by ~0.025 μmol/l, as observed in experiments (49, 51).

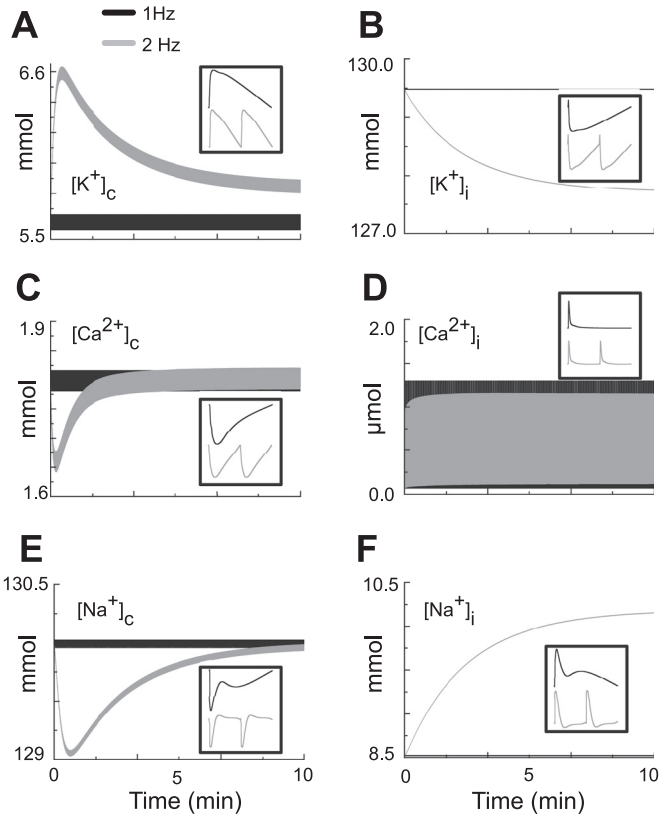

Fig. 5. Evaluation of the ability of the model to maintain ionic stability when paced at either 1 or 2 Hz (10 min of simulation shown). The *insets* in *A–F* are the selected ion concentrations as they change during a single AP when the model is paced at either 1 or 2 Hz. *A*: $[K^+]_c$. *B*: $[K^+]_i$. *C*: $[Ca^{2+}]_c$. *D*: $[Ca^{2+}]_i$. *E*: $[Na^+]_c$. *F*: $[Na^+]_i$.

The hAMr model reveals a critical difference with the original model of Nygren et al. in terms of long-term stability of both intracellular and cleft space ion concentrations. The elimination of the constant background flux $\Phi_{Na,en}$ allows the hAMr model to adhere to fundamental physical principles of conservation of charge and ionic species, which results in the existence of long-term mathematical steady states (25). Moreover, the changes in intracellular and cleft ionic concentrations with an increase in pacing frequency to 2 Hz in the hAMr model are consistent with rate-dependent concentration alterations observed in experiments (40).

AP Morphology

Figure 6*A* shows the AP waveform generated by our model and the original Nygren et al. model at a rate of 1 Hz. The change to the hAMr model AP was relatively small; the AP in our model had a more rapid rate of late repolarization. We note that in the Nygren et al. model, the AP morphology was tuned to match a subset of recorded data almost exactly. In the hAMr model, in contrast, we chose not to make this requirement upon the AP morphology. This is because recorded traces from human atrial myocytes, even when from the same region of the atria, as shown in Fig. 6*B* (from the right atrial appendage; unpublished observations by U. Ravens, used with permission), often show heterogeneity in AP morphology from one patient to the next. Thus, rather than require adherence to a single experimental recording, we chose to focus on the reproduction of key kinetic properties of individual K^+ currents while also requiring AP morphological features that fall well within the range of experimental observations in human atrial myocytes.

Early Repolarization of the AP

Figure 7 shows early repolarization of the AP in our model. In Fig. 7*A*, APs from both the Nygren et al. (40) and hAMr models are shown. The AP upstroke and early repolarization are emphasized. The major changes in our model were *1*) an increased AP upstroke velocity and *2*) a slight decrease in the rate of early repolarization, as indicated by the dashed arrows. The increased rate of rise of the AP is a result of an increase in peak I_{Na}, as discussed previously; the slight decrease in the rate of early repolarization in the hAMr model can be attributed to the alteration in the net contribution of I_t and I_{Kur}. Figure 7*B*

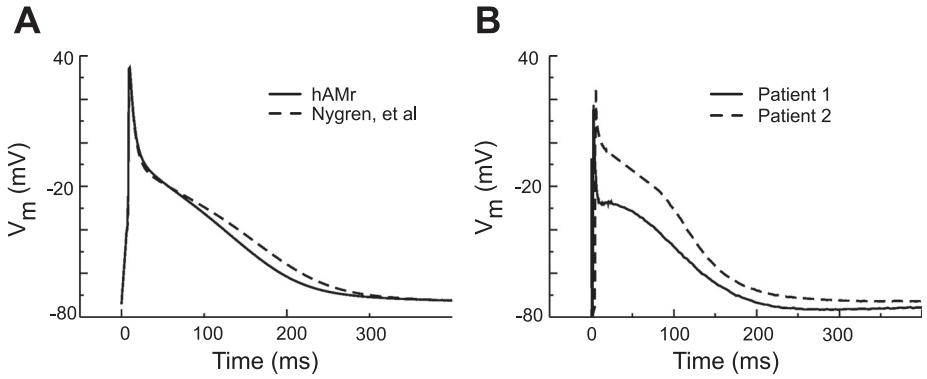

Fig. 6. *A*: APs generated by the hAMr and Nygren et al. (40) models. *B*: APs recorded from human atrial myocytes from two different patients (unpublished data from U. Ravens, used with permission) in response to a 1-Hz stimulus train at 37°C. V_m, transmembrane voltage.

shows I_t during the first 50 ms of the cardiac AP for both hAMr and Nygren et al. (40) models. I_t activated more quickly in our hAMr formulation. This was due to the increased rate of rise of the AP; peak I_t density was also larger. In contrast, the peak density of I_{Kur} (Fig. 7*C*) was decreased, and the inactivation of this current was slower in the hAMr model than in the original model.

Figure 7*D* shows the sum of I_t and I_{Kur}. Although each of the two currents were significantly different in the models, their sum was quite similar. In the hAMr model, the sum of I_t and I_{Kur} decayed more rapidly and thus resulted in a slightly slower early repolarization. Figure 7*E* shows the roles of g_t and g_{Kur} on APD_{30}; g_t and g_{Kur} are expressed as percentages of the nominal g_t and g_{Kur}, defined as those in the hAMr model. Note that this AP

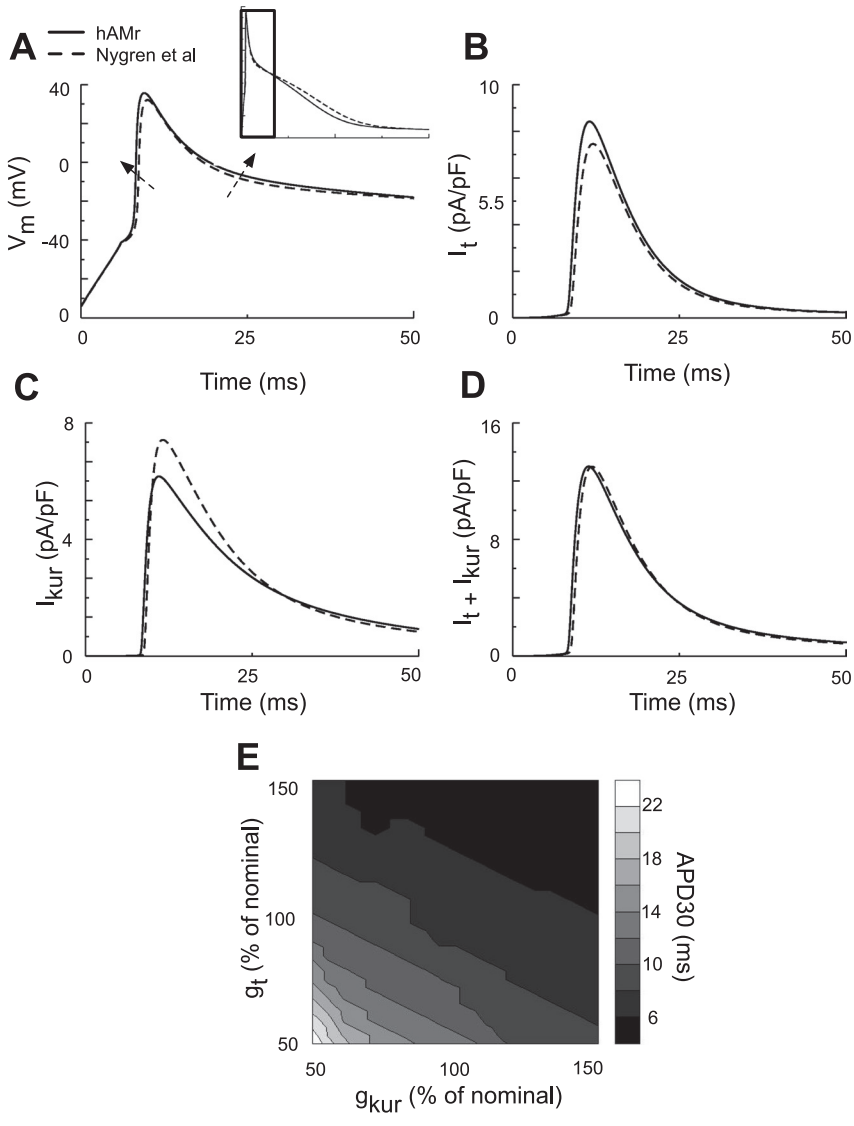

Fig. 7. Illustration of early AP repolarization in the hAMr model and in the model of Nygren et al. (40). *A*: comparison of AP morphology during early repolarization in the two models. The *inset* shows the time course of portion of the AP examined. *B* and *C*: traces of both I_t and I_{Kur} during the first 50 ms of a single AP. *D* and *E*: contribution of I_t and I_{Kur} to early repolarization of the human atrial AP. *D*: sum of I_t and I_{Kur}, which was similar for the hAMr and Nygren et al. (40) models. *E*: APD_{30} as a function of g_t and g_{Kur}; nominal values are those used in the hAMr model.

property is dependent on both g_t and g_{Kur}; for instance, if g_t and g_{Kur} are both decreased by 25%, the APD_{30} lengthens by ~6 ms; if both g_t and g_{Kur} increase by 25%, the APD_{30} decreases by ~1 ms. Early repolarization in the hAMr model is thus especially sensitive to the collective decrease in I_t and I_{Kur}.

Late Repolarization of the AP

Figure 8 shows the revised simulation of late repolarization of the AP. Figure 8*A* shows AP traces during late repolarization for each model. The *inset* shows the entire time course of the APs, whereas the box indicates the latter 150 ms of the cardiac cycle. The major waveform change in the hAMr model compared with the original model of Nygren et al. was an increased rate of late repolarization, as shown by the dashed arrow. I_{K1} is shown during the entire time course of the AP in Fig. 8*B* (the box indicates the last 150 ms of the AP). Although the densities of I_{K1} in early repolarization were quite similar between the two models, the density of I_{K1} in our modified formulation was, on average, ~12% greater than that of the parent model during late repolarization. This corresponds to a difference in the average current density of ~0.06 pA/pF during the last 150 ms of the AP between the two models. Figure 8*C* shows I_{Kur} during late repolarization of the AP. Note that I_{Kur} during late repolarization was decreased in the hAMr model. I_{Kur} was ~24% smaller on average in the hAMr model; the difference in average current density during the time course

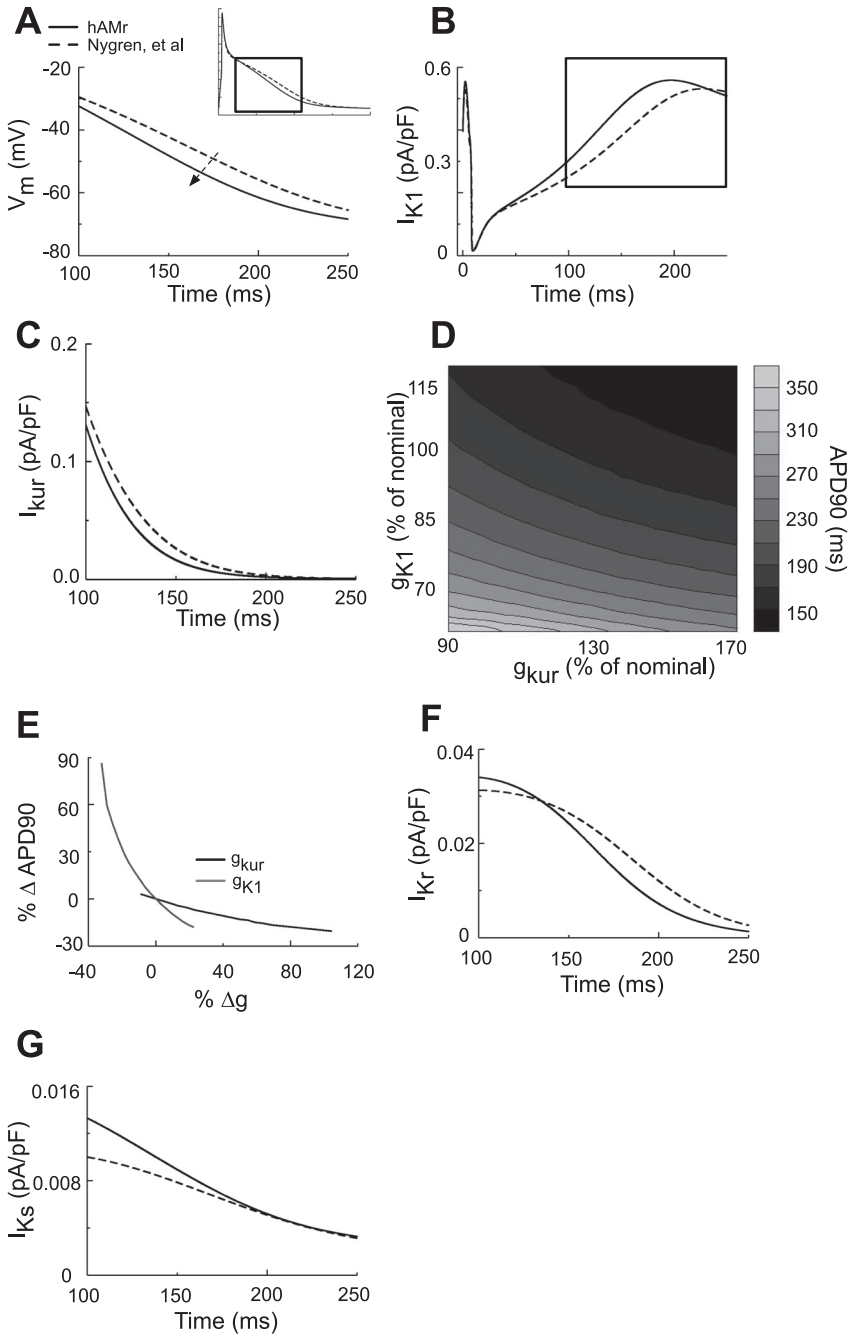

Fig. 8. AP waveform of the human atrial myocyte during late repolarization. *A*: late repolarization occurred more rapidly in the hAMr model compared with the model of Nygren et al. (40), as shown by the arrow. *B*: note that I_{K1} during late repolarization in the hAMr model was increased compared with the model of Nygren et al. (40). *C*: I_{Kur} during the late repolarization phase of the AP. The magnitude and time courses of I_{Kur} in the hAMr and Nygren et al. (40) models were very similar. *D*: modulation of the time course of late repolarization as a function of the relative conductance of g_{K1} and g_{Kur}. *E*: percent change in APD_{90} with changes in g_{K1} or g_{Kur} compared with nominal values (those used in the hAMr model). The relative size and time course of the two additional K^+ currents active during late repolarization in the human atrial myocyte (I_{Kr} and I_{Ks}) are shown in *F* and *G*, respectively. Note the small density of these currents compared with I_{K1} and I_{Kur} in *B* and *C*.

shown was ~0.007 pA/pF. Although it was an order of magnitude smaller than I_{K1} during late repolarization, the density of I_{Kur} can have a marked influence on APD_{90}.This is shown in Fig. 8*D*. Here, g_{K1} and g_{Kur} are expressed as percentages of nominal g_{K1} and g_{Kur} in the hAMr model. APD_{90} is dependent on both g_{K1} and g_{Kur}, as shown in Fig. 8*E*. Note that a decrease in g_{Kur} (from its nominal value) has a greater influence on increases in APD_{90} compared with a similar increase in g_{Kur} (and subsequent APD_{90} decreases). For nominal g_{K1}, a 10% decrease in the nominal value of g_{Kur} causes an increase in APD_{90} on the order of 10 ms, whereas a 30% increase in nominal g_{Kur} is necessary to lengthen the AP by the same amount. Deviations from the nominal value in g_{K1} exert a greater influence on APD_{90} than g_{Kur}. However, similarly to g_{Kur}, increases in g_{K1} from its nominal value exert less influence on APD_{90} than decreases: for a nominal g_{Kur}, a 15% decrease and increase in g_{K1} will increase and decrease APD_{90} by ~20 and ~10 ms, respectively.

In addition to I_{K1} and I_{Kur}, the role of smaller K^+ conductances was examined during late repolarization of the AP. Figure 8*F* shows the role of I_{Kr} (human *ether-a-go-go*-related gene) during late repolarization; the density of this current was ~31% smaller for the interval of 150–250 ms from the beginning of a single cardiac cycle. However, this corresponds to a difference in the average density of I_{Kr} in the two models of only ~0.004 pA/pF (~0.5% of total membrane current) during the same time course. I_{Ks} (Fig. 8*G*) was ~14% greater in the hAMr model until 200 ms of the AP; this was only a difference of ~0.001 pA/pF (~0.2% of total membrane current) in the average current density between the two models for the same time course.

Rate Dependence of the hAMr Model

Figure 9 shows the rate dependence of key parameters in our new model compared with experimental data. For reference, we also show the rate dependence of the same parameters in the Nygren et al. model (40). In Fig. 9, *A* and *B*, peak I_t and end-pulse (as measured at the end of the voltage clamp) I_{Kur} were normalized to the peak and step current density, respectively, for a stimulation frequency of 0.1 Hz. Figure 9*A* shows the rate dependence of peak I_t compared with the experimental data of Fermini et al. (16). I_t as formulated in the original Nygren et al. model (dashed trace) was strongly rate dependent.The reformulation of recovery kinetics in the hAMr model resulted in much less rate dependence of I_t (black trace), resulting in a close match to experimental data. Figure 9*B* shows the rate dependence of end-pulse I_{Kur} compared with the experimental results of Feng et al. (15). The alteration of inactivation kinetics in the hAMr model improved the representation of the rate dependence of I_{Kur}.The new formulation reduced the amount of available I_{Kur} after an increase in pacing rate (15). The rate dependence of APD_{30} together with data from the experiments by Dawodu et al. [black "X"s (8)] are shown in Fig. 9*C*. APD_{30} was normalized to its value at a basic cycle length of 1,600 ms for the model of Nygren et al., the hAMr model, and the experimental data. While the original model qualitatively replicated the experimental observation that APD_{30} increases in response to an increase in stimulation rate, the present simulations more closely reproduced experimental results. The rate dependence of APD_{90} is shown in Fig. 9*D* and was compared with experiments (8, 9). APD_{90} was normalized to its value at a rate of 1,200 ms. The rate dependence of APD_{90} in the hAMr model was a much closer match to the available experimental values; moreover, in the hAMr model, APD_{90} continued to decrease for pacing rates of >2 Hz, a behavior that has been observed in experiments but was not duplicated by the previous model (40). It is important to note that there was a close agreement between experimental measurements and the improved rate dependence. This is an

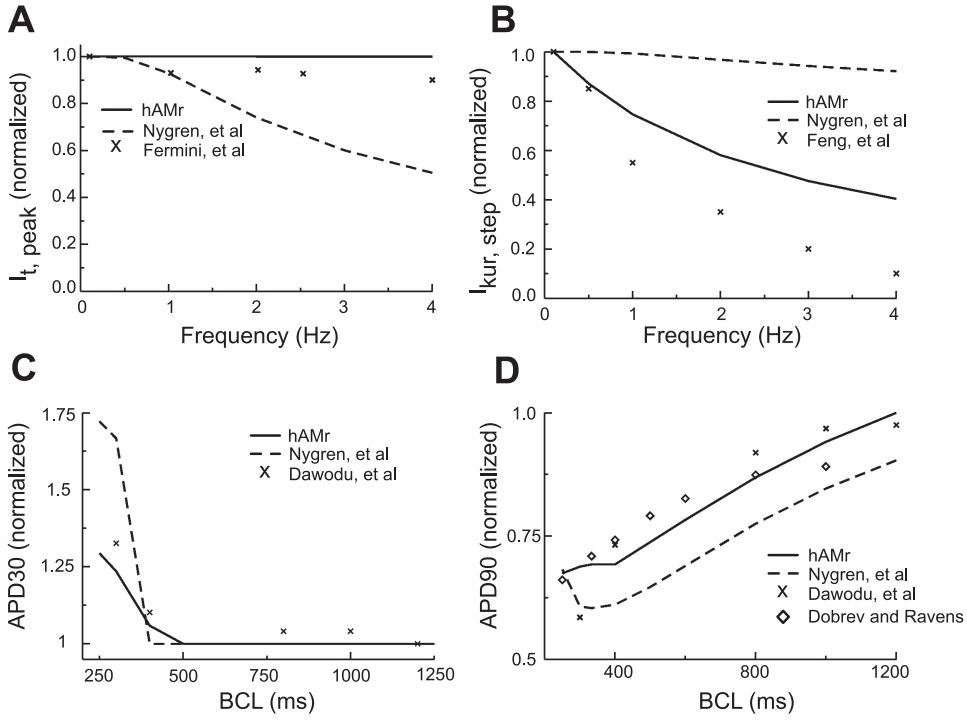

Fig. 9. Changes in K^+ currents and APD as a function of basic cycle length (BCL). *A*: rate dependence of normalized peak I_t for both models and experimental data (16). From a holding potential of −60 mV, 100 steps to 0 mV of 200-ms duration were applied at frequencies of 0.1, 0.5, 1, 2, 3, and 4 Hz. The voltage-clamp protocol was identical for the experiment and simulation. *B*: rate dependence of normalized I_{Kur} at the end of test voltage pulses for both models and experimental data (15). From a holding potential of −80 mV, 100 steps to +40 mV of 200-ms duration were applied at frequencies of 0.1, 0.5, 1, 2, 3, and 4 Hz. The voltage-clamp protocol was identical for the experiment and simulation. *C*: rate dependence of APD_{30} in both models compared with the experiment (8). *D*: rate dependence of APD_{90} in both models compared with experiments (8, 9).

emergent feature of the hAMr model rather than a pattern of behavior to which the model was fit (see DISCUSSION).

Utility of the hAMr Model in Applications

Unlike other models of the human atrial myocyte, the hAMr model features new repolarization kinetics and rate dependence and thus is appropriate for a wide range of cellular, tissue-level, and organ-level studies of the APs in human atria under normal and pathophysiological conditions. Of particular utility at the cellular level is the simulation of pharmacological interventions. Figure 10 shows the results of the use of the hAMr model to reproduce the effects of the $I_t/I_{Kur}/I_{K(ACh)}$ blocker AVE0118 on human atrial myocyte APs, as described by Christ et al. (6). For sinus rhythm (or healthy) atrial myocyte APs, simulations used the hAMr model, whereas for chronic atrial fibrillation APs, a version of the hAMr model modified to represent chronic atrial fibrillation based on experimental findings (6, 9) was used. The experimentally measured effects of AVE0118 on diverse K^+ currents (6) were used in both sets of simulations. The simulations reproduced experimental findings (6) showing that AVE0118 administered in cells at sinus rhythm increased APD_{20} but not APD_{90}, whereas in cells with chronic atrial fibrillation, both APD_{20} and APD_{90} increased with the administration of AVE0118. The increase in APD_{90} afforded by AVE0118 in human atrial myocytes with chronic atrial fibrillation has been suggested to underlie the efficacy of this compound to convert atrial fibrillation to sinus rhythm in goats (2), but the potential effects in a clinical setting to treat atrial fibrillation is unknown. As a forerunner and complement to clinical testing, the hAMr model could prove a useful tool to investigate the tissue-level effects of AVE0118 as well as numerous other pharmacokinetic therapies targeting human atrial myocytes.

DISCUSSION

The primary goal of the present study was to provide a computational framework in which the repolarization of the human atrial myocyte could be examined. This was achieved via the development of a new human atrial myocyte model based on the model of Nygren et al. (40), which incorporated recent experimental K^+ current data and then characterized the emergent rate dependence of the new model. The results presented here demonstrate the ways in which select properties of major repolarizing K^+ currents can result in the ability of the model to reproduce experimental measurements of AP properties of adult human atrial myocytes. In addition, the RMP matches available experimental data from human atrial myocytes. Importantly, our model now satisfies fundamental physical constraints of conservation of charge and ionic species and thereby ensures unique, long-term steady states of ionic concentrations in both the intracellular and cleft spaces.The morphology of the AP in the hAMr model resembles experimental APs from adult human atrial myocytes. This is the case despite the fact that no attempt was made to systematically match any such recordings. APD values for both early and late repolarization more closely approximated those measured in experiments, and an emergent feature of the hAMr model is its improved rate dependence of both individual currents and APD. The model presented in this article provides insight into repolarization processes and results in a much-improved match of current and AP behaviors to available experiments, an essential characteristic for the future use of the model in the context of human atrial rhythm disturbances.

I_{K1} and RMP

I_{K1} is essential for the maintenance of the resting potential in all myocytes and for late repolarization (17, 43). This is true even though the conductance of I_{K1} in the atria (compared with the ventricles) is relatively small (30). Some studies have indicated that I_{K1} in the atria does not exhibit strong rectification, i.e., the current-voltage relation shows little, if any, negative slope (30). These studies would suggest that, at high levels of depolarization, I_{K1} would maintain a current density close to its maximum value at less depolarized potentials and would remain at this density throughout the time course of the AP. It is possible that limitations in methodology (i.e., seal resistance changes for human atrial myocytes) lead to leakage currents, which may be interpreted as incomplete rectification but are an experimental artifact (39). A strong rectification of I_{K1} allows the reproduction of experimentally observed current densities and the maintenance of a stable RMP and has thus been included in the hAMr model.

One important consequence of the relatively small conductance of I_{K1} in the human atria is a slower rate of final repolarization as well as a somewhat more depolarized RMP (~5–10 mV) compared with human ventricular myocytes (45). The RMP maintained in the hAMr model is −74.0 mV, which agrees with the majority of experimental studies using isolated adult human atrial myocytes (8, 21, 45, 46, 52, 60). The model of Courtemanche et al. (7) of the human atrial myocyte has a relatively hyperpolarized RMP of −81.2 mV. This is more typical of the maximum diastolic potential found in recordings from isolated human atrial tissue preparations (20, 45). We believe that accurate representation of the RMP is important

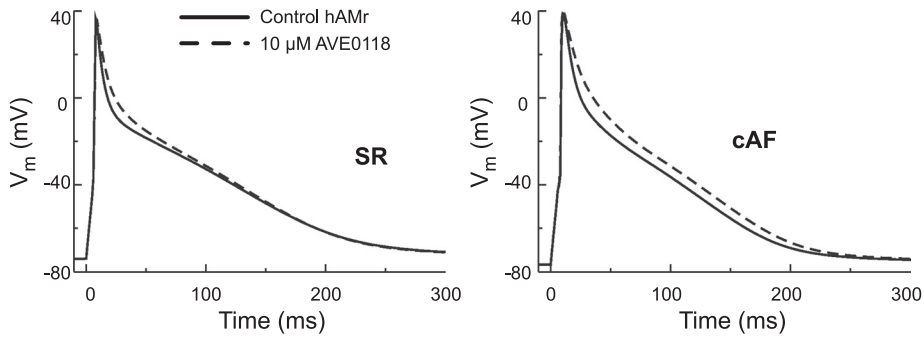

Fig. 10. Use of the hAMr model to investigate the effects of the drug AVE0118 on the human atrial AP waveform during sinus rhythm (SR) and chronic atrial fibrillation (cAF). The specific differential effects of AVE0118 in SR versus cAF human atrial myocytes described by Ref. 6 are shown here, illustrating the potential utility of the hAMr model in the simulation of pharmacological interventions.

not only in the context of steady-state phenomena but in the case of rate accommodation, wherein the maximum diastolic potential is typically depolarized compared with RMP and may affect both the availability and time dependence of ionic currents.

Demonstration of Long-term Pacing and Steady-State Ion Concentrations in the hAMr Model

Intracellular and cleft ion concentrations are at steady states for >10 min of simulation at a pacing rate of 1 Hz in the hAMr model. A small but notable change occurs in the steady-state value of $[K^+]_c$ in the hAMr model compared with the original model of Nygren et al. (40); basal diastolic $[K^+]_c$ was increased to 5.6 from 5.4 mmol/l (~3.7% increase). This may be explained as resulting from the elimination of Φ_{Na} in the hAMr model: the stimulus current that enters the intracellular space is now carried by potassium ions (24). These potassium ions are then extruded via sarcolemmal ion channels and accumulate in the cleft space surrounding the cell, whereas the bulk K^+ concentration remains unchanged. Experimental measurements of extracellular ion concentrations are taken from the bulk fluid surrounding the cell or preparation, and there may exist locally higher concentrations of ions in an extracellular cleft space surrounding a myocyte than may be measured in the bulk plasma.

When the stimulation frequency was increased to 2 Hz, $[K^+]_c$ accumulated, increased to values up to ~1 mmol/l greater than its basal value (~18% increase), and then returned to a unique steady state close to its initial value. $[Na^+]_c$ and $[Ca^{2+}]_c$ initially decreased by ~0.8% and ~8%, respectively, and then returned to steady-state values. At a stimulation rate of 2 Hz, $[Na^+]_i$ increased by ~18% to a new steady-state value. $[K^+]_i$ reached a new steady-state value, which was a 1.5% decrease. $[Ca^{2+}]_i$, in contrast, underwent very little change in steady-state value at a stimulation rate of 2 Hz: the peak magnitude of the transient was decreased by ~6% (peak magnitude), and peak diastolic $[Ca^{2+}]_i$ increased. It is difficult to provide a comprehensive comparison of our results due of the lack of experimental data for many of these quantities. However, an increase in $[K^+]_c$ with an increase in stimulation rate to 2 Hz has been recorded in experiments (31). In addition, peak diastolic $[Ca^{2+}]_i$ has also been shown to increase with an increase in stimulation frequency in experimental models (49, 51).

The elimination of Φ_{Na} results in the existence of a mathematical steady state in the hAMr model, as discussed briefly in Jacquemet et al. (25). The concentration of nonspecific, monovalent cations in the intracellular space, constant for any stimulation protocol in the hAMr model, was ~138.4 mmol/l. Based on the elegant stability analysis provided in Jacquemet et al. (25), it can be determined that the initial condition for the transmembrane potential (initial condition in the APPENDIX) in the hAMr model ensures that the system is dynamically stable for any stimulation protocol.

AP Waveforms

The AP in the hAMr model is characterized by a slightly slowed early (phase 1) repolarization as well as a more rapid late (phase 3) repolarization compared with the model of Nygren et al. (40) and fits well within the range of AP morphologies seen in recordings from experiments with adult human atrial myocytes (U. Ravens, unpublished observations). It is well known that there exist heterogeneities in human atrial AP shape. AP morphology and characteristics can vary both from patient to patient and from region to region in the atria (45) and have variously been classified into "types" or patterns (8, 10, 27, 57). Rather than require that the resultant AP morphology adhere to a specific experimental recording as in previous models of the adult human atrial myocyte (7, 40), we have chosen to arrive at a morphology for which accurate reproduction of observed behaviors of individual currents has been the focus. Although an exact match to an atrial AP shape was not required in our development, the result of the hAMr model is an AP morphology that is markedly similar to many experimental traces.

Repolarization Reserve Revisited

In the human atrial myocyte, I_t and I_{Kur}, followed by I_{K1}, are the main time- and voltage-dependent currents responsible for repolarization. I_t is active during phase 1 (early) repolarization of the AP only, whereas I_{Kur} inactivates very slowly and thus contributes to repolarization during phases 1, 2, and 3 of the human atrial AP. I_{K1} figures prominently during late repolarization; because of the small densities of I_{Kr} and I_{Ks} compared with I_{K1}, neither current plays a major role during late repolarization in the hAMr model.

In the human atria, myocytes may have a relatively small safety factor for repolarization due to decreased densities of outward currents compared with ventricular myocytes. "Repolarization reserve" has previously been defined as the ability of myocardial cells to repolarize when normal repolarizing currents are altered or reduced via either physiological perturbations or pathological challenges (22). This concept has been applied as a measure of the safety factor for repolarization (17) and, in practice, has been defined as the sum of the K^+ currents I_{K1}, I_{Kr}, and/or I_{Ks}, which can be activated under physiological conditions (17). However, the concept needs to be operationally defined with reference to particular contexts and situations. For example, outward currents that are active relatively late in the cardiac cycle may compensate for the low availability of other repolarizing currents when pacing rates increase, due to residual activation (i.e., I_{Kur}). The comparatively low density of outward K^+ currents in the human atrial myocyte may result in low repolarization reserve, particularly in the context of drug therapies and pathologies that may interfere with K^+ currents and repolarization processes. The underlying complexity of outward current remodeling, which contributes to varying degrees of the repolarization reserve, has been demonstrated recently (44). These new findings highlight the dynamic nature of the repolarization reserve and suggest that even outward currents active in early repolarization, i.e., I_t and I_{Kur}, may be critically important for repolarization in the human atria.

Rate Response of the AP Waveform

As shown in Fig. 9, the rate dependence of both I_t and I_{Kur} agree closely with experimental data. In addition, the frequency dependence of the AP waveform in the present model reproduces recent experimental results (Fig. 9) (8, 9).This improved representation of current availability and AP behavior at a variety of pacing rates is essential not only for the

simulation of behaviors in healthy tissue but for the capacity of the model to lend its predictive power to disease state phenomena.

It is of interest to simulate the behavior of atrial myocytes and tissue at increased rates of stimulation so that atrial tachycardic rhythm disturbances (such as atrial flutter and atrial fibrillation) can be examined. For instance, in both paroxysmal and chronic atrial fibrillation, structural remodeling including progressive fibrosis has been widely implicated in the initiation and maintenance of the arrhythmia (3, 11). However, despite a wealth of investigation in recent years (29, 34, 48), a complete picture of the mechanisms underlying fibrosis-linked atrial arrhythmia has yet to emerge. Recent investigations have suggested that a critical aspect of atrial fibrotic remodeling may be functional: electrotonic coupling between fibroblasts and myocytes may play a crucial role at the cellular level (4, 5, 19, 26, 28, 35, 37, 38). Fibroblasts that are present within and maintain the extracellular matrix adjacent to myocytes can have a large influence on local myocyte activation and repolarization. To appropriately address questions regarding the potential involvement of electronic coupling between fibroblasts and human atrial myocytes in the development and maintenance of atrial arrhythmias, it is essential that the repolarization processes of the latter cell type be realistically represented at a variety of physiological and pathophysiological stimulation rates. The hAMr model was used in a recent study from our group (36) to investigate the effects of fibroblast-myocyte coupling on excitability and repolarization in the adult human atrial myocyte under a variety of conditions, including increased rates of stimulation.

Limitations of This Study

There are important limitations to the present work that should be recognized.

In Fig. 3*D*, computational traces of the sum of I_t and I_{Kur} appear to decay more rapidly than the experimental voltage clamp results. A cause of this apparent disparity is that the experimental traces available are from a recent publication (21), which, however, was not used in the new model, as the focus of the study of Gluais et al. was characterization of the AP and steady-state current density properties of human atrial myocytes after treatment with risperidone compared with control. The experimental datasets used to formulate the kinetics included in the model (15, 56) unfortunately did not include multiple voltage-clamp traces of the currents and thus could not be presented for a comparison to the simulated data shown in Fig. 3*D*.

The use of Hodgkin-Huxley formalism in our model employs first-order kinetics. Activation/deactivation and inactivation/recovery from inactivation are each governed by a single time constant, obtained, where possible, from fits to experimental measurements at a variety of holding potentials. However, many of these processes exhibit very complex kinetics. Markovian models allow for the existence of a multiplicity of channel states, each with specific transitional rate constants; however, these rate constants are often very difficult to determine. In addition, Markovian models often result in comprehensive AP models that are computationally expensive, particularly when more than one channel is involved. Additionally, Markovian models for the ion channels in the human atrium that were the main focus of this study (I_t and I_{Kur}) have not yet been developed. Future development and incorporation of such models will lead to further accuracy in the representation of ionic currents.

The mathematical formulations that account for Ca^{2+} homeostasis in the model of Nygren et al. (40) remained unchanged in the hAMr model. Although detailed models of Ca^{2+} cycling have emerged in recent years (23, 47), such models focus on ventricular rather than atrial tissue. Because of the lack of appropriate experimental data and because incorporation of a detailed model of Ca^{2+} cycling may be computationally prohibitive, particularly with respect to tissue and organ models, the formulation of Ca^{2+} cycling used in the model of Nygren et al. (40) was maintained in the hAMr model.

APPENDIX: MODEL EQUATIONS

This section contains all the equations, parameter values, and initial conditions necessary to be the basis for a full and accurate implementation of the hAMr model when combined with the kinetic descriptions available in the model of Nygren et al. (40). Unless otherwise noted, the units are as follows: time (in s), voltage (in mV), concentrations (in mmol/L), current (in pA), conductance (in nS), capacitance (in pF), volume (in nl), and temperature (in K). The stimulus used to evoke an AP was a rectangular current pulse (I_{stim}) with amplitude of 280 pA and duration of 6 ms.

I_t

$$I_t = g_t \times r \times s\,(V - E_K)$$
$$dr/dt = (r_\infty - r)/\tau_r$$
$$ds/dt = (s_\infty - s)/\tau_s$$
$$r_\infty = 1.0/[1.0 + e^{(V\,-\,1.0)/-11.0}]$$
$$s_\infty = 1.0/[1.0 + e^{(V\,+\,40.5)/11.5}]$$
$$\tau_s = 0.025635 \times e^{\{-[(V\,+\,52.45)/15.8827]2\}} + 0.01414$$
$$\tau_r = 0.0035 \times e^{[-(V/30.0)2]} + 0.0015$$

I_{Kur}

$$I_{Kur} = g_{Kur} \times a_{ur} \times i_{ur} \times (V - E_K)$$
$$da_{ur}/dt = (a_{ur,\infty} - a_{ur})/\tau_{aur}$$
$$di_{ur}/dt = (i_{ur,\infty} - i_{ur})/\tau_{iur}$$
$$a_{ur,\infty} = 1.0/[1.0 + e^{-(V\,+\,6)/8.6}]$$
$$i_{ur,\infty} = 1.0/[1.0 + e^{(V\,+\,7.5)/10.0}]$$
$$\tau_{aur} = 0.009/[1.0 + e^{(V\,+\,5.0)/12.0}] + 0.0005$$
$$\tau_{iur} = 0.59/[1.0 + e^{(V\,+\,60.0)/10.0}] + 3.05$$

Intracellular Ion Concentrations

$$d[K^+]_i/dt = -[I_t + I_{Kur} + I_{K1} + I_{Ks} + I_{Kr} - 2(I_{NaK}) + I_{stim}]/(Vol_i \times F)$$
$$d[Na^+]_i/dt = -[I_{Na} + I_{BNa} + 3(I_{NaCa}) + 3(I_{NaK})]/(Vol_i \times F)$$

Parameter Values

$$k_{Ca} = 0.025 \text{ mmol/l}$$
$$I_{NaK,max} = 68.55 \text{ pA}$$

Maximum Conductance Values

$$P_{Na} = 0.0018 \text{ nl/s}$$
$$g_t = 8.25 \text{ nS}$$
$$\text{Mean } g_{Kur} = 2.25 \text{ nS}$$
$$g_{K1} = 3.1 \text{ nS}$$

Initial Conditions

$$V = -74.0320 \text{ mV}$$
$$[Na^+]_c = 130.0221 \text{ mmol/l}$$

$[K^+]_c = 5.5602$ mmol/l
$[Ca^{2+}]_c = 1.8158$ mmol/l
$[Na^+]_i = 8.5168$ mmol/l
$[K^+]_i = 129.4860$ mmol/l
$[Ca^{2+}]_i = 6.5000 \times 10^{-5}$ mmol/l
$[Ca^{2+}]_d = 7.1000 \times 10^{-5}$ mmol/l
$[Ca^{2+}]_{rel} = 0.6326$ mmol/l
$[Ca^{2+}]_{up} = 0.6492$ mmol/l
$m = 3.2890 \times 10^{-3}$
$h_1 = 0.8772$
$h_2 = 0.8739$
$d_L = 1.4000 \times 10^{-5}$
$f_{L1} = 0.9986$
$f_{L2} = 0.9986$
$r = 1.0890 \times 10^{-3}$
$s = 0.9486$
$a_{ur} = 3.6700 \times 10^{-4}$
$i_{ur} = 0.9673$
$n = 4.3740 \times 10^{-3}$
$p_a = 5.3000 \times 10^{-5}$
$F_1 = 0.4701$
$F_2 = 0.0028$
$O_C = 0.0268$
$O_{Calse} = 0.4315$
$O_{TC} = 0.0129$
$O_{TMgC} = 0.1904$
$O_{TMgMg} = 0.7145$

ACKNOWLEDGMENTS

The authors gratefully acknowledge Prof. Ursula Ravens and members of her laboratory for providing action potential recording data from human atrial myocytes. These are included in Fig. 4*B*.

GRANTS

The laboratory of N. A. Trayanova gratefully acknowledges support of this work by National Heart, Lung, and Blood Institute Grants R01-HL-063195, R01-HL-082729, and R01-HL-067322 and National Science Foundation Grant CBET-0601935. The W. R. Giles laboratory is funded by the Canadian Institutes of Health Research and the Heart and Stroke Foundation of Canada. In addition, W. Giles holds a Medical Scientist Award from the Alberta Heritage Foundation for Medical Research.

REFERENCES

1. **Amos GJ, Wettwer E, Metzger F, Li Q, Himmel HM, Ravens U.** Differences between outward currents of human atrial and subepicardial ventricular myocytes. *J Physiol* 491: 31–50, 1996.
2. **Blaauw Y, Schotten U, van Hunnik A, Neuberger HR, Allessie MA.** Cardioversion of persistent atrial fibrillation by a combination of atrial specific and nonspecific class III drugs in the goat. *Cardiovasc Res* 75: 89–98, 2007.
3. **Burstein B, Nattel S.** Atrial fibrosis: mechanisms and clinical relevance in atrial fibrillation. *J Am Coll Cardiol* 51: 802–809, 2008.
4. **Camelliti P, Devlin GP, Matthews KG, Kohl P, Green CR.** Spatially and temporally distinct expression of fibroblast connexins after sheep ventricular infarction. *Cardiovasc Res* 62: 415–425, 2004.
5. **Camelliti P, McCulloch AD, Kohl P.** Microstructured cocultures of cardiac myocytes and fibroblasts: a two-dimensional in vitro model of cardiac tissue. *Microsc Microanal* 11: 249–259, 2005.
6. **Christ T, Wettwer E, Voigt N, Hala O, Radicke S, Matschke K, Varro A, Dobrev D, Ravens U.** Pathology-specific effects of the $I_{Kur}/I_{to}/I_{K,ACh}$ blocker AVE0118 on ion channels in human chronic atrial fibrillation. *Br J Pharmacol* 154: 1619–1630, 2008.
7. **Courtemanche M, Ramirez RJ, Nattel S.** Ionic mechanisms underlying human atrial action potential properties: insights from a mathematical model. *Am J Physiol Heart Circ Physiol* 275: H301–H321, 1998.
8. **Dawodu AA, Monti F, Iwashiro K, Schiariti M, Chiavarelli R, Puddu PE.** The shape of human atrial action potential accounts for different frequency-related changes in vitro. *Int J Cardiol* 54: 237–249, 1996.
9. **Dobrev D, Ravens U.** Remodeling of cardiomyocyte ion channels in human atrial fibrillation. *Basic Res Cardiol* 98: 137–148, 2003.
10. **Escande D, Loisance D, Planche C, Coraboeuf E.** Age-related changes of action potential plateau shape in isolated human atrial fibers. *Am J Physiol Heart Circ Physiol* 249: H843–H850, 1985.
11. **Everett TH, Olgin JE.** Atrial fibrosis and the mechanisms of atrial fibrillation. *Heart Rhythm* 4: S24–S27, 2007.
12. **Fabiato A, Fabiato F.** The two components of the human atrial action potential. *Circ Res* 29: 296–305, 1971.
13. **Fedida D, Wible B, Wang Z, Fermini B, Faust F, Nattel S, Brown AM.** Identity of a novel delayed rectifier current from human heart with a cloned K^+ channel current. *Circ Res* 73: 210–216, 1993.
14. **Feng J, Wang Z, Li GR, Nattel S.** Effects of class III antiarrhythmic drugs on transient outward and ultra-rapid delayed rectifier currents in human atrial myocytes. *J Pharmacol Exp Ther* 281: 384–392, 1997.
15. **Feng J, Xu D, Wang Z, Nattel S.** Ultrarapid delayed rectifier current inactivation in human atrial myocytes: properties and consequences. *Am J Physiol Heart Circ Physiol* 275: H1717–H1725, 1998.
16. **Fermini B, Wang Z, Duan D, Nattel S.** Differences in rate dependence of transient outward current in rabbit and human atrium. *Am J Physiol Heart Circ Physiol* 263: H1747–H1754, 1992.
17. **Fink M, Giles WR, Noble D.** Contributions of inwardly rectifying K^+ currents to repolarization assessed using mathematical models of human ventricular myocytes. *Philos Transact A Math Phys Eng Sci* 364: 1207–1222, 2006.
18. **Firek L, Giles WR.** Outward currents underlying repolarization in human atrial myocytes. *Cardiovasc Res* 30: 31–38, 1995.
19. **Gaudesius G, Miragoli M, Thomas SP, Rohr S.** Coupling of cardiac electrical activity over extended distances by fibroblasts of cardiac orgin. *Circ Res* 93: 421–428, 2003.
20. **Gelband H, Bush HL, Rosen MR, Myerburg RJ, Hoffman BF.** Electrophysiologic properties of isolated preparations of human atrial myocardium. *Circ Res* 30: 293–300, 1972.
21. **Gluais P, Bastide M, Grandmougin D, Fayad G, Adamantidis M.** Risperidone reduces K^+ currents in human atrial myocytes and prolongs repolarization in human myocardium. *Eur J Pharmacol* 497: 215–222, 2004.
22. **Han W, Chartier D, Li D, Nattel S.** Ionic remodeling of cardiac Purkinje cells by congestive heart failure. *Circulation* 104: 2095–2100, 2001.
23. **Hinch R, Greenstein JL, Tanskanen AJ, Xu L, Winslow RL.** A simplified local control model of calcium-induced calcium release in cardiac ventricular myocytes. *Biophys J* 87: 3723–3736, 2004.
24. **Hund TJ, Kucera JP, Otani NF, Rudy Y.** Ionic charge conservation and long-term steady state in the Luo-Rudy dynamic cell model. *Biophys J* 81: 3324–3331, 2001.
25. **Jacquemet V.** Steady-state solutions in mathematical models of atrial cell electrophysiology and their stability. *Math Biosci* 208: 241–269, 2007.
26. **Jacquemet V, Henriquez CS.** Loading effect of fibroblast-myocyte coupling on resting potential, impulse propagation, and repolarization: insights from a microstructure model. *Am J Physiol Heart Circ Physiol* 294: H2040–H2052, 2008.
27. **Jakob H, Oelert H, Rupp J, Nawrath H.** Functional role of cholinoceptors and purinoceptors in human isolated atrial and ventricular heart muscle. *Br J Pharmacol* 97: 1199–1208, 1989.
28. **Kohl P, Camelliti P, Burton F, Smith G.** Electrical coupling of fibroblasts and myocytes: relevance for cardiac propagation. *J Electrocardiol* 38: 45–50, 2005.
29. **Kostin S, Klein G, Szalay Z, Hein S, Bauer EP, Schaper J.** Structural correlate of atrial fibrillation in human patients. *Cardiovasc Res* 54: 361–379, 2002.
30. **Koumi S, Backer CL, Arentzen CE.** Characterization of inwardly rectifying K^+ channel in human cardiac myocytes. Alterations in channel behavior in myocytes isolated from patients with idiopathic dilated cardiomyopathy. *Circulation* 92: 164–174, 1995.
31. **Kunze DL.** Rate-dependent changes in extracellular potassium in the rabbit atrium. *Circ Res* 41: 122–127, 1977.
32. **Lagrutta A, Wang J, Fermini B, Salata JJ.** Novel, potent inhibitors of human Kv1.5 K^+ channels and ultrarapidly activating delayed rectifier potassium current. *J Pharmacol Exp Ther* 317: 1054–1063, 2006.
33. **Lindblad DS, Murphey CR, Clark JW, Giles WR.** A model of the action potential and underlying membrane currents in a rabbit atrial cell. *Am J Physiol Heart Circ Physiol* 271: H1666–H1696, 1996.

34. **Luo MH, Li YS, Yang KP.** Fibrosis of collagen I and remodeling of connexin 43 in atrial myocardium of patients with atrial fibrillation. *Cardiology* 107: 248–253, 2007.
35. **MacCannell KA, Bazzazi H, Chilton L, Shibukawa Y, Clark RB, Giles WR.** A mathematical model of electrotonic interactions between ventricular myocytes and fibroblasts. *Biophys J* 92: 4121–4132, 2007.
36. **Maleckar MM, Greenstein JL, Giles WR, Trayanova NA.** Electrotonic coupling between human atrial myocytes and fibroblasts alters myocyte excitability and repolarization. *Biophys J*. In press.
37. **Miragoli M, Gaudesius G, Rohr S.** Electrotonic modulation of cardiac impulse conduction by myofibroblasts. *Circ Res* 98: 801–810, 2006.
38. **Miragoli M, Salvarani N, Rohr S.** Myofibroblasts induce ectopic activity in cardiac tissue. *Circ Res* 101: 755–758, 2007.
39. **Newell EW, Schlichter LC.** Integration of K^+ and Cl^- currents regulate steady-state and dynamic membrane potentials in cultured rat microglia. *J Physiol* 567: 869–890, 2005.
40. **Nygren A, Fiset C, Firek L, Clark JW, Lindblad DS, Clark RB, Giles WR.** Mathematical model of an adult human atrial cell: the role of K^+ currents in repolarization. *Circ Res* 82: 63–81, 1998.
41. **Olson TM, Alekseev AE, Liu XK, Park S, Zingman LV, Bienengraeber M, Sattiraju S, Ballew JD, Jahangir A, Terzic A.** Kv1.5 channelopathy due to KCNA5 loss-of-function mutation causes human atrial fibrillation. *Hum Mol Genet* 15: 2185–2191, 2006.
42. **Radicke S, Cotella D, Graf EM, Banse U, Jost N, Varro A, Tseng GN, Ravens U, Wettwer E.** Functional modulation of the transient outward current I_{to} by KCNE beta-subunits and regional distribution in human non-failing and failing hearts. *Cardiovasc Res* 71: 695–703, 2006.
43. **Rasmusson RL, Clark JW, Giles WR, Shibata EF, Campbell DL.** A mathematical model of a bullfrog cardiac pacemaker cell. *Am J Physiol Heart Circ Physiol* 259: H352–H369, 1990.
44. **Roden DM.** Repolarization reserve: a moving target. *Circulation* 118: 981–982, 2008.
45. **Schram G, Pourrier M, Melnyk P, Nattel S.** Differential distribution of cardiac ion channel expression as a basis for regional specialization in electrical function. *Circ Res* 90: 939–950, 2002.
46. **Shibata EF, Drury T, Refsum H, Aldrete V, Giles W.** Contributions of a transient outward current to repolarization in human atrium. *Am J Physiol Heart Circ Physiol* 257: H1773–H1781, 1989.
47. **Shiferaw Y, Watanabe MA, Garfinkel A, Weiss JN, Karma A.** Model of intracellular calcium cycling in ventricular myocytes. *Biophys J* 85: 3666–3686, 2003.
48. **Spach MS, Heidlage JF, Dolber PC, Barr RC.** Mechanism of origin of conduction disturbances in aging human atrial bundles: experimental and model study. *Heart Rhythm* 4: 175–185, 2007.
49. **Stefenelli T, Wikman-Coffelt J, Wu ST, Parmley WW.** Intracellular calcium during pacing-induced ventricular fibrillation. Effects of lidocaine. *J Electrocardiol* 25: 221–228, 1992.
50. **Tessier S, Karczewski P, Krause EG, Pansard Y, Acar C, Lang-Lazdunski M, Mercadier JJ, Hatem SN.** Regulation of the transient outward K^+ current by Ca^{2+}/calmodulin-dependent protein kinases II in human atrial myocytes. *Circ Res* 85: 810–819, 1999.
51. **Thandroyen FT, Morris AC, Hagler HK, Ziman B, Pai L, Willerson JT, Buja LM.** Intracellular calcium transients and arrhythmia in isolated heart cells. *Circ Res* 69: 810–819, 1991.
52. **Trautwein W, Kassebaum DG, Nelson RM, Hecht HH.** Electrophysiological study of human heart muscle. *Circ Res* 10: 306–312, 1962.
53. **Wang S, Bondarenko VE, Qu Y, Morales MJ, Rasmusson RL, Strauss HC.** Activation properties of Kv4.3 channels: time, voltage and $[K^+]_o$ dependence. *J Physiol* 557: 705–717, 2004.
54. **Wang S, Bondarenko VE, Qu YJ, Bett GC, Morales MJ, Rasmusson RL, Strauss HC.** Time- and voltage-dependent components of Kv4.3 inactivation. *Biophys J* 89: 3026–3041, 2005.
55. **Wang Y, Xu H, Kumar R, Tipparaju SM, Wagner MB, Joyner RW.** Differences in transient outward current properties between neonatal and adult human atrial myocytes. *J Mol Cell Cardiol* 35: 1083–1092, 2003.
56. **Wang Z, Feng J, Shi H, Pond A, Nerbonne JM, Nattel S.** Potential molecular basis of different physiological properties of the transient outward K^+ current in rabbit and human atrial myocytes. *Circ Res* 84: 551–561, 1999.
57. **Wang Z, Fermini B, Nattel S.** Delayed rectifier outward current and repolarization in human atrial myocytes. *Circ Res* 73: 276–285, 1993.
58. **Wang Z, Fermini B, Nattel S.** Sustained depolarization-induced outward current in human atrial myocytes. Evidence for a novel delayed rectifier K^+ current similar to Kv1.5 cloned channel currents. *Circ Res* 73: 1061–1076, 1993.
59. **Wang Z, Yue L, White M, Pelletier G, Nattel S.** Differential distribution of inward rectifier potassium channel transcripts in human atrium versus ventricle. *Circulation* 98: 2422–2428, 1998.
60. **Workman AJ, Kane KA, Rankin AC.** The contribution of ionic currents to changes in refractoriness of human atrial myocytes associated with chronic atrial fibrillation. *Cardiovasc Res* 52: 226–235, 2001.
61. **Zhang H, Garratt CJ, Zhu J, Holden AV.** Role of up-regulation of I_{K1} in action potential shortening associated with atrial fibrillation in humans. *Cardiovasc Res* 66: 493–502, 2005.